NIH Public Access
Author Manuscript
*Planta*. Author manuscript; available in PMC 2014 October 06.

Published in final edited form as:
*Planta*. 2009 March ; 229(4): 731–745. doi:10.1007/s00425-008-0868-0.

# Reciprocal chromosome translocation associated with TDNA-insertion mutation in Arabidopsis: genetic and cytological analyses of consequences for gametophyte development and for construction of doubly mutant lines

**Marc J. Curtis**[1], **Katia Belcram**[2], **Stephanie R. Bollmann**[1], **Colin M. Tominey**[1], **Peter D. Hoffman**[1], **Raphael Mercier**[2], and **John B. Hays**[1]

[1]Department of Environmental and Molecular Toxicology, Oregon State University, Corvallis, OR, USA

[2]UMR254, INRA, Route de Saint-Cyr, 78026 Versailles Cedex, France

## Abstract

Chromosomal rearrangements may complicate construction of Arabidopsis with multiple TDNA-insertion mutations. Here, crossing two lines homozygous for insertions in *AtREV3* and *AtPOLH* (chromosomes I and V, respectively) and selfing F1 plants yielded non-Mendelian F2 genotype distributions: frequencies of +/++/+ and *1/1 2/2* progeny were only 0.42 and 0.25%. However, the normal development and fertility of double mutants showed *AtPOLH-1* and *AtREV3-2* gametes and *1/1 2/2* embryos to be fully viable. F2 distributions could be quantitatively predicted by assuming that F1 selfing produced inviable (*1,2*) and (+,+) gametophytes 86% of the time. Some defect intrinsic to the F1 selfing process itself thus appeared responsible. In selfing *AtREV3* $^{+/2}$ single mutants, imaging of ovules and pollen showed arrest or abortion, respectively, of half of gametophytes; however, gametogenesis was normal in *AtREV3* $^{2/2}$ homozygotes. These findings, taken together, suggested that T-DNA insertion at *AtREV3* on chromosome I had caused a reciprocal I–V translocation. Spreads of meiosis I chromosomes in selfing *AtREV3* $^{+/2}$ heterozygotes revealed the predicted cruciform four-chromosome structures, which fluorescence in situ hybridization showed to invariably include both translocated and normal chromosomes I and V. Sequencing of the two junctions of T-DNA with *AtREV3* DNA and the two with gene At5g59920 suggested translocation via homologous recombination between independent inverted-repeat T-DNA insertions. Thus, when crosses between TDNA-insertion mutants yield anomalous progeny distributions, TDNA-linked translocations should be considered.

### Keywords

Arabidopsis; Gametophyte development; Reciprocal translocation; T-DNA; Translesion synthesis polymerase

## Introduction

Sophisticated genetic analyses are increasingly being employed to elucidate complex phenomena in Arabidopsis. Rine (2005) has noted that “although the analysis of single and

NIH-PA Author Manuscript
NIH-PA Author Manuscript
NIH-PA Author Manuscript

NIH-PA Author Manuscript

NIH-PA Author Manuscript

NIH-PA Author Manuscript

double (yeast) mutants has proven useful, there is nothing quite as revealing as the phenotypes of the right triple mutant, unless of course it is the critical quadruple mutant." In Arabidopsis the availability of hundreds of thousands of lines marked by TDNA-insertion mutations would seem to make construction of double-mutant and even triple-mutant lines quite straightforward. However, chromosomal rearrangements are often induced during T-DNA insertion. In some TDNA-mutant screens, up to 17% of the insertion mutants showed chromosomal rearrangements (Castle et al. 1993). TDNA-induced inversions and translocations have been described (Nacry et al. 1998; Laufs et al. 1999; Tax and Vernon 2001; Lafleuriel et al. 2004). Such chromosomal rearrangements often do not impart an obvious phenotype and thus go unnoticed. However, in genetic crosses segregation of parental loci within the rearranged chromosomes may cause progeny distributions to markedly deviate from Mendelian expectations (Patterson 1978). Inversions would reduce recombination within the inverted chromosomal regions and translocations would change linkage groups. These distortions can only be recognized when genetically tracking two loci.

Tolerance of UVB-induced DNA damage by the translesion synthesis polymerases Pol η and Pol ζ was previously studied in irradiated Arabidopsis roots, using mutants in which the respective genes, *AtPOLH*and *AtREV3*, had been disrupted by T-DNA insertion (Curtis and Hays 2007). When crossing the single mutants (*AtPOLH-1* and *AtREV3-2*) to construct a double mutant for the studies, we observed highly non-Mendelian distributions of genotypes among the F2 progeny of selfed F1 double heterozygotes.

Such abnormal progeny distributions might reflect specific genotype effects on gametophyte development, during which roughly half of Arabidopsis genes are expressed (Honys and Twell 2004). Alternatively, the selfing process itself might generate inviable gametes in a genotype-specific manner. For example, aberrant meiosis engendered by reciprocal translocations involving T-DNA insertions associated with specific mutations might produce gametes lacking portions of chromosomes. The absence of genes located on these missing chromosome regions might affect gametophyte development, even if the TDNA-insertion mutations did not.

Previous investigations of translocations in Arabidopsis were incomplete in one or more respects, so did not integrate a comprehensive set of phenomena into a complete picture. Here we describe quantitative analyses of the (non-Mendelian) distributions of genotypes among F2 progeny of selfed F1 *AtPOLH* $^{+/1}$ *AtREV3* $^{+/2}$ double-heterozygotes and of the (Mendelian) distributions among F3 progeny of selfed (*1/1 +/2*) and (*+/1 2/2*) F2 plants. These progeny distributions could be quantitatively explained simply by assuming loss of double-mutant and double-wt ovules and pollen, mitigated by a single meiotic cross-over that allowed 14% of both to survive. Selfing *AtPOLH* $^{+/1}$ *AtREV3* $^{+/2}$ double-heterozygotes did show post-meiotic ovule arrest and pollen abortion. Loss of double-mutant and double-wt gametes is consistent with a reciprocal translocation involving chromosome V (*AtPOLH* linkage group) and chromosome I (*AtREV3* linkage group). Analyses of meiotic-chromosomal spreads by microscopy and chromosome-specific fluorescence in situ hybridization (FISH) supported this hypothesis. Broader implications of translocation via apparent TDNA–TDNA homologous recombination for construction of multiply mutant lines are considered.

NIH-PA Author Manuscript

NIH-PA Author Manuscript

NIH-PA Author Manuscript

## Materials and methods

### Growth and plant crosses

Arabidopsis lines AtREV3-2/2 (SALK_029237) and AtPOLH-1/1 (SALK_129731) were previously isolated (Curtis and Hays 2007) from the respective T3 seed populations, generated by the Salk Institute Genomic Analysis Laboratory and obtained from the Arabidopsis Biological Resource Center. F1 *AtPOLH*$^{+/1}$ *AtREV3*$^{+/2}$ double heterozygotes were derived from manual fertilization of AtREV3-2/2 ovules by*AtPOLH-1/1* pollen. For segregation analyses, progeny of selfed F1 or F2 double heterozygotes were genotyped using PCR analyses (see Identification of genotypes). All plants were routinely grown in a Percival PGC-105 growth chamber maintained at 22°C, under cool white fluorescent lights (Phillips F72T12/CW/VHO, 16/8 h photoperiod, output of 80 μmol $m^{-2}$ $s^{-1}$).

### Identification of genotypes

Genotypes were determined by PCR analysis of genomic DNA extracted from single leaves, as previously described (Curtis and Hays 2007). Gene-specific primers for *AtREV3* were 5′-CCT TGC ATC ATC TCA ATG ACG GCT CC-3′ (Ra5′ primer) and 5′-CGA GCT GCA CGT TTT GAC TTC C-3′ (Ra3′primer). *AtPOLH* gene-specific primers were 5′-CAT TCT ATG TGT TGT CGC TGC AGG TGG-3′ (5′primer) and 5′-CCT TGT TAT GGG CTA TGC CAG CAG AAC-3′ (3′primer). For tracking insertion lines, respective gene-specific PCR primers were used with a primer specific to the left-border of the SALK T-DNA (5′-CCA CCC CAG TAC ATT AAA AAC GTC CGC-3′).

### Imaging of gametophyte development

Inflorescence tissues were fixed in FAA (3.7% formalin, 5% acetic acid, 50% ethanol) overnight at 4°C, as described by Siddiqi et al. (2000). The fixed tissue was rinsed once with 50% ethanol and then dehydrated by washing successively with a series of acetone solutions (50, 75, 90 and 100%), for 15 min each. The tissue was then incubated for 2 h in methyl benzoate and overnight in a 7:1 (v/v) mixture of methyl benzoate with Spurr's resin (MBSR suspension). Ovules were dissected with tungsten needles under a dissecting microscope onto a glass slide. Dissected ovules were mounted in MBSR suspension under a coverslip and examined using a Leica DMRB microscope (Leica Microsystems, Wetzler, Germany) with differential-interference-contrast optics.

Inflorescence tissue for dissection of anthers was fixed with FAA (see above), rinsed once in 1× phosphate-buffered saline (PBS): 137 mM NaCl, 2.7 mM KCl, 4.3 mM $Na_2HPO_4$ and 1.4 mM $KH_2PO_4$, pH 7.3), and washed overnight in a solution of 1% Tween detergent in 1× PBS. Anthers were then stained overnight with 10 μM Hoechst dye in 0.04% Tween/0.02× PBS. Pollen grains were released into 40% glycerol using tungsten needles, mounted under coverslips and imaged with the Leica DMRB epifluorescence microscope. The epifluorescence microscope was fitted with a mercury lamp and an appropriate filter set (Chroma Technology Corp., Rockingham, VT, USA) for imaging Hoechst 33342 dye (filter set 11000v3: UV). Epifluorescence images were captured using a CoolSNAP-Pro digital camera operated using Image Pro PLUS software (MediaCybernetics, Silver Spring, MD, USA).

NIH-PA Author Manuscript

NIH-PA Author Manuscript

NIH-PA Author Manuscript

## Cytology

Spreading of meiocyte chromosomes was carried out as described in (Grelon et al. 2001). The FISH was performed according to (Lysak et al. 2006). A 9 kb clone containing 18S-5, 8S-25S *Triticum aestivum* rDNA (pTa71 (Gerlach and Bedbrook 1979)) and two BACs from the short arm of chromosome V (F7J8, F2I11) were labeled by digoxigenin nick translation mix according to the manufacturer's instructions (Roche, Nutley, NJ, USA) and were detected by mouse anti-digoxigenin antibodies (Roche), rabbit anti-mouse FITC and goat anti-rabbit Alexa-488 antibodies (Molecular Probes, Eugene, OR, USA). A 3.5-kb fragment of 5S *A. thaliana* rDNA (pCT4.2; Campell et al. 1992) and two BACs from the chromosome III (F8J2, T4P13) were labeled by biotin nick translation mix according the manufacturer's instruction (Roche) and detected by Avidin-Texas Red and goat biotinylated anti-avidin D antibodies (Vector laboratories, Orton Southgate, Peterborough, UK). All observations were made using a Leica (Leica Microsystems) DMRXA2 microscope; photographs were taken using a CoolSNAP HQ (Roper Scientific, Tucson, AZ, USA) camera driven by Open-LAB 4.0.4 software; all images were further processed with OpenLAB4.0.4 or AdobePhotoshop 7.0 (http://www.adobe.com).

## Mapping of T-DNA junctions

T-DNA/genomic junctions were mapped using adapter-ligation-mediated PCR (“anchored-PCR”) as described by O'Malley et al. (2007), with modifications. Briefly, genomic *AtREV3 2*/2 DNA (200 ng), 0.28 μM “Eco” Adapter DNA, and 0.28 μM “Hind” adapter DNA were digested with 50 U *Eco*RI endonuclease (New England Biolabs, Ipswich, MA, USA) and 5 U *Hin*dIII endonuclease (Invitrogen, Carlsbad, CA, USA) in the presence of 5 U T4 DNA-ligase (Invitrogen) for 6 h at 37°C in 1× T4 ligase buffer [40 mM Tris–HCl (pH 7.8 at 25°C), 10 mM $MgCl_2$, 10 mM dithiothreitol, 0.5 mM ATP (Fermentas, Glen Burnie, MD, USA)]. Adapter ligation was completed in a thermocycler: 37°C for 10 s, 10°C for 10 s, repeat for 198 cycles and finished with 20 min at 65°C.

The adapter-ligated genomic DNA (1 μl) was the template for PCR using primers LBa1 and AP1 (O'Malley et al. 2007) in 1× *Taq* buffer [50 mM KCl, 10 mM Tris– HCl (pH 9.0 at 25°C), 1.5 mM $MgCl_2$, 0.1% Triton X-100] with 1 U *Taq* polymerase (GenScript, Piscataway, NJ, USA). PCR amplification was carried out for 10 cycles at 96°C for 20 s and 72°C for 140 s, followed by 15 cycles at 96°C for 20 s and 67°C for 140 s. PCR reactions were diluted 1:5 in distilled $H_2O$; 1.5 μl of the diluted product was used as the template for a second (“nested”) PCR reaction using primers LBb1 and AP2 (O'Malley et al. 2007): 5 cycles at 96°C for 30 s, 94°C for 20 s and 72°C for 140 s, followed by 23 cycles at 96°C for 20 s, 67°C for 20 s and 72°C for 130 s.

Products from the nested PCR reaction were cloned in vector pCR®4 using a TOPO TA Cloning Kit for Sequencing (Invitrogen) and transformed into chemically competent *E. coli* DH5α by standard procedures. Twelve individual colonies were isolated and plasmid DNA was purified using a QIAprep Spin Miniprep Kit (Qiagen, Valencia, CA, USA). Purified plasmids were sequenced using both T3- and T7-promoter primers.

NIH-PA Author Manuscript NIH-PA Author Manuscript NIH-PA Author Manuscript

The junction of the 3′end of *APP2C* with the CEN side of the T-DNA (as shown in Fig. 6) was PCR amplified using primer *P3′* (5′-CAA ATC TCC TCC TCC AAC CA-3′) and a TDNA-specific primer (5′-TTT GGG TGA TGG TTC ACG TA-3′). The extent of T-DNA leftwards (as shown in Fig. 6) from the junction of the 5′ end of *AtREV3* with the RETEL side of the T-DNA was PCR amplified using primer *Rb5′* (5′-AAA GCG TTT TCC CTT ACG AA-3′) and a TDNA-specific primer (5′-GGC ATG CAC ATA CAA ATG GA-3′). The extent of T-DNA rightwards from the junction of the 3′ end of *AtREV3* with the CEN side of the T-DNA was PCR amplified using primer *Rb3′* (5′-GGC CTG AAA TCT GAG ACA GC-3′) and a TDNA-specific primer (5′-AGA CAA TCG GCT GCT CTG AT-3′).

## Results

### Anomalous segregation of progeny of selfed *AtPOLH*$^{+/1}$ *AtREV3*$^{+/2}$ double heterozygotes

The double heterozygotes selfed were either F1 progeny from crosses of *AtPOLH* $^{1/1}$ with *AtREV3* $^{2/2}$ homozygous mutants, or F2 progeny from the F1 selfing. PCR genotyping of hundreds of progeny plants showed selfing of both F1 (Table 1) and F2 (Supplementary Table 1) *AtPOLH* $^{+/1}$ *AtREV3* $^{+/2}$ double heterozygotes to yield similarly skewed distributions. Of 1,189 total progeny from several selfings of*AtPOLH* $^{+/1}$ *AtREV3* $^{+/2}$ F1 or F2 double heterozygotes, only three double mutants and five wild-type progeny were recovered. Because *AtPOLH* is on Arabidopsis chromosome V and *AtREV3* is on chromosome I, the genes should normally assort independently. Three genotypes were overrepresented while six were underrepresented. Closer analysis revealed interesting correlations between progeny distributions and inferred parental-gamete genotypes (Fig. 1). The severely underrepresented (*1/1 2/2*and +/++/+) progeny genotypes (Fig. 1, dotted boxes) can only arise from unions of genetically identical double-mutant male and female gametes, both (*1,2*) or both (+,+). The strongly overrepresented (*1/1* +/+ and +/+ *2/2*) progeny genotypes (solid boxes) must arise from unions of genetically identical single-mutant gametes, both (*1,* +) or both (+, *2*); neither of their parental gametes can be double-mutant or double-wt. The moderately underrepresented (*1/1 2/* +,+ */1 2/2, +/1* +/+, and +/++/*2*) progeny must be derived from unions of double-mutant (*1,2*) or (+,+) gametes with single-mutant (*1,* +) or (+,*2*) gametes. Finally, the modestly overrepresented (*+/1 +/2*) progeny can be derived both from unions of (*1,* +) and (+,*2*) gametes with one another and from unions of two (*1,2*) double-mutant gametes with (+,+). These correlations directed our attention to possible deficiencies in the genesis and/or viability of (+,+) and (*1,2*) gametes.

Table 1 (and Supplementary Table 1) show the observed genotype distributions to differ dramatically from Mendelian expectations (“Expect 1”): very low probability ($P < 0.005$, Chi-square test) that the differences are due to chance. The data do correspond reasonably well to the prediction (“Expect 2”) for a hypothetical case in which the average yields of double wild-type and double mutant gametes were sharply reduced, so as to produce 6:6:44:44 (*1,2*: + ,+:*1,* + : +,*2*) gamete-frequency distributions (in contrast to the normal 25:25:25:25); the small deviations between observed and Expect 2 may be due to chance ($P > 0.10$). Other hypothesized gamete ratios predicted progeny distributions that fitted our observations less well. For example, comparison of progeny distribution to that expected for *1,2* and +,+ gamete frequencies of 5% yields a Chi-square value of 21.4, while comparison

NIH-PA Author Manuscript

NIH-PA Author Manuscript

NIH-PA Author Manuscript

to 7% yields a Chi-square value of 15.4. For 6%, the Chi-square value was 11.2 (Supplementary Table 1).

The observed non-Mendelian distribution is not due to unequal production or detection of allele-specific PCR products used for genotyping. Table 2 and Supplementary Table 2 demonstrate closely similar PCR detection of the four alleles (within 6–8%). Table 2 also shows that no *AtPOLH* or *AtREV3* progeny genotype, considered in isolation, is inherently inviable: the respective single-locus genotypes are present in the progeny population at Mendelian frequencies. Furthermore, closer inspection of Table 1 (and Supplementary Table 1) shows that abnormally low detection of any one of the four alleles (*AtREV3*+, for example) among one class of progeny homozygous at the second locus (*AtPOLH* +/+ in this example) is always balanced by abnormally high detection among the other class of progeny homozygous at the second locus (*AtPOLH* $^{1/1}$ in this example).

The observation that wt (+/+ +/+) genotypes are as rare among progeny of selfed double F1 heterozygotes as double mutant (*1/1 2/2*) genotypes suggests already that the non-Mendelian distribution is not due to intrinsic inviability of *AtREV3-2* or *AtPOLH-1* alleles but is inherent in the selfing process. Furthermore, *1/1 2/*2 double mutants were recovered at Mendelian frequencies among F3 progeny of selfed F2 *AtPOLH* $^{+/1}$ *AtREV3* $^{2/2}$ and selfed F2 *AtPOLH* $^{1/1}$ *AtREV3* $^{+/2}$ single heterozygotes (Curtis and Hays 2007). Thus, even the double-null mutant appears to be fully viable in embryo.

Table 1 (“Expect 2” column) shows the observed F2 genotype distribution to be fitted reasonably well by simply assuming that some event(s) associated with meiosis in *AtPOLH* $^{+/1}$ *AtREV3* $^{+/2}$ double heterozygotes caused yields of (+,+) and (*1, 2*) gamete frequencies to be reduced sevenfold. Although male gametes are typically in large excess, loss of female gametes would reduce the number of ovules available for fertilization, and consequently reduce seed set. In fact, selfing F2 *AtPOLH* $^{+/1}$ *AtREV3* $^{+/2}$plants show reduced seed set (23.5 ± 4.7) versus wild type (44 ± 10.1). However, so do selfing *AtPOLH*$^{1/1}$ *AtREV3* $^{+/2}$ and *AtPOLH* $^{+/+}$ *AtREV3* $^{+/2}$ F2 plants (21.4 ± 4.2 and 24 ± 5.0, respectively). All F2 plants *not* heterozygous at the *AtREV3* locus, regardless of *AtPOLH* genotype, showed normal seed set (not shown). Thus, reduced seed set was specific to *AtREV3* $^{+/2}$ heterozygosity. To further investigate this phenomenon, which we suspected might be related to the observed non-Mendelian distributions of the progeny of selfed double heterozygotes, we analyzed *AtREV3* $^{+/2}$ single heterozygotes.

## Analyses of progeny of selfed *AtREV3 +/2* heterozygotes

A heterozygous *AtREV3* $^{+/2}$ plant was identified among the original SALK T3 population and self-fertilized. Its progeny were scored for seed set (Table 3). Seed set was reduced in all of 27 *AtREV3* $^{+/2}$ progeny, to approximately half that of the wild type or homozygous-mutant (*2/2*) progeny. Such 50% reduction in seed set was previously seen in heterozygous mutants defective in female reproductive development (Drews et al. 1998). Completely infertile *homozygotes* are typical for such mutants, but here seed sets of selfed *AtREV3* $^{2/2}$ homozygotes and selfed wild-type plants were similar (Table 3, column 3). Among these, all siliques sampled from all +/+ plants and all siliques sampled from 10 of 12 *2/2* plants appeared normal (Table 3, column 4, < 35 seeds); 1 of 5 or 2 of 5 siliques sampled from two

NIH-PA Author Manuscript

NIH-PA Author Manuscript

NIH-PA Author Manuscript

*2/2* plants showed reduced seed set. Importantly, the *AtREV3* $^{+}$ and *AtREV3-2* alleles were equally represented even among the reduced numbers of progeny of selfed *AtREV3* $^{+/2}$ heterozygotes (Table 4). This contrasts with the reduced transmission of the *AtREV3-2* allele that would be expected if it specifically affected female gamete development. The significance of this Mendelian distribution among the reduced progeny of selfed *AtREV3* $^{+/2}$ heterozygotes (Table 4) is considered below under "Reciprocal translocation associated with the *AtREV3-2* TDNA-insertion."

To test more completely for equal transmission of both mutant and wild-type alleles, we performed reciprocal crosses between wild-type (Col-0) and *AtREV* $^{+/2}$ parents. All of the six crosses between randomly selected single anthers from *AtREV3* $^{+/2}$ plants and wt carpels yielded similar frequencies of +/+ and *+/2* progeny (mean 19 ± 5 and 17 ± 3, respectively). Similarly, all six crosses between wild-type (+) anthers and randomly selected carpels from *AtREV3* $^{+/2}$ plants yielded approximately equal numbers of +/+ and $^{+/2}$ progeny (mean, 11 ± 2 and 12 ± 4, respectively). Thus, in *AtREV3* $^{+/2}$ heterozygotes there was no discrimination against mutant (*AtREV3-2*) pollen or ovaries per se, despite the reduced seed set.

## Ovule development in *AtREV3* $^{+/2}$ heterozygotes

We next used imaging techniques to follow ovule development. Inspection of the developing seeds in young, fertilized ovaries (siliques) of selfed *AtREV3* $^{+/2}$ heterozygotes showed roughly half to be normal; the other "seeds" were smaller, suggesting that they were actually unfertilized ovules (data not shown). We then dissected ovules out from ovaries in flower buds at different stages of development and viewed them by whole-mount microscopy (Fig. 2). All defined stages of ovule development (Schneitz et al. 1995) were unambiguously identified. After completion of meiosis, a single cell is selected to divide (stage 2-IV, arrow) and the other three meiotic products degenerate (stage 2-IV, arrowhead). Frames in Fig. 2 show nuclei (white arrows) produced by the three mitotic divisions of ovules: two nuclei (stage 3-II/III), four nuclei (stage 3-IV), and eight nuclei (stage 3-V). After the third mitotic division one nucleus on each side of the large central vacuole migrates to the center of the embryo sac. The embryo sac then matures by fusion of the two central nuclei and cellularization of these and the remaining nuclei, forming seven cells (stage 3-VI). At this stage the three antipodal nuclei degenerate (stage 3-VI, dashed circle).

To compare ovule development in wild type, *AtREV3* $^{2/2}$ nullizygous and *AtREV3* $^{+/2}$ heterozygous plants, ovules were dissected from a consecutive series of flower buds of increasing size (six buds per inflorescence), analyzed by whole-mount microscopy and scored for developmental stage (Fig. 3). The smallest buds (approximately floral stage 11) define *Bud size no. 1* and the largest (floral stage 13) *Bud size no. 6* (Fig. 3a–f). Supplementary Figures 1, 2 and 3 show the fractions of ovules at each stage in each of two to five individual buds of each size (no. 1 through no. 6) from +/+, *2/2*, and *+/2* plants, respectively. Figure 3 shows the summed distributions for +/+, *2/2* and *+/2* buds of each size. Progression through meiosis and the initial degeneration of all but one nucleus (stage 2-IV/V) appeared similar for all three genotypes (note in Fig. 3a–c the rough coincidence or near-coincidence of the distributions of ovules). Notably, ovules from the smallest buds of *+/2* heterozygotes showed no obvious deficiencies relative to +/ + and *2/2*. (The small

NIH-PA Author Manuscript

NIH-PA Author Manuscript

NIH-PA Author Manuscript

differences among the average distributions seen in Fig. 3a–c are similar to differences seen for individual buds with the same genotype (Supplementary Figures 2a–c, 3a–c and 4a–c), so are not considered significant. However *size no. 4* buds showed marked differences between ovules from +/+ and *2/2* homozygotes (means of 94 and 92% ovules, respectively had completed the first round of gametophyte mitosis) versus ovules from +/2 heterozygotes (only 14% had completed mitosis, with 62% at stage 3-I). In *size no. 6* buds of +/2 heterozygotes, ~ 50% of the ovules were at stage 3-I and still resembled those shown in Fig. 2 (stage 3-I), with no sign of degeneration. The remaining ovules in these *size no. 6* buds were fully matured, stage 3-VI. During normal stage 3-I, the gamete genome is copied and separated by mitosis into two nuclei, whose presence defines the gametophyte to be at stage 3-II. Thus, ovules from *+/2* heterozygotes were arrested at approximately stage 3-I, either prior to genome replication or the first gametophyte mitosis.

## Pollen development in *AtREV3* $^{+/2}$ heterozygotes

To determine whether or not the deficiency in reproductive development in *AtREV3* $^{+/2}$ plants extended to male gametes as well, the primary inflorescences from two, three and four wild-type, *AtREV3* $^{2/2}$ and*AtREV3* $^{+/2}$ individuals, respectively, were fixed and then stained with the chromatin-binding Hoechst dye. Three anthers were removed from each of 11-12 consecutive flower buds per plant. Pollen was dissected from individual anthers for imaging by differential-interference or epifluorescence microscopy (Fig. 4). Tetrads initially formed in *AtREV3* $^{+/2}$ heterozygotes appeared similar to those in A*tREV3* $^{2/2}$ and wt homozygotes (Fig. 4a–f). No *AtREV3* $^{+/2}$ plants produced dyads or other aberrant spores, suggesting that meiosis and spore-cell-wall formation were normal. Pollen released from tetrads at this stage appeared normal (not shown). However, degenerating pollen were subsequently observed in anthers from *AtREV3* $^{+/2}$ plants only [compare Fig. 4 k, l (arrow) to g–j], by the time the prominent pollen vacuole was absorbed. At this developmental stage, gametes have not undergone the first round of mitosis, as indicated by the presence of single nuclei. Analysis of 5,409, 5,630 and 6,832 pollen grains showed degeneration of 41% of pollen in *AtREV3* $^{+/2}$ anthers, but <1% degeneration of pollen in wild-type or*AtREV3* $^{2/2}$ anthers, respectively. After the first round of gamete mitosis (Fig. 4 m–r), 42% of pollen imaged in *AtREV3* $^{+/2}$ anthers was collapsed (Fig. 4q, arrow), but <1% were collapsed in wild-type or*AtREV3* $^{2/2}$ anthers. The non-collapsed pollen in *AtREV3* $^{+/2}$ anthers at this stage did show the two nuclei (Fig. 4r, arrowheads), indicative of mitotic division, as did all wild-type and *AtREV3* $^{2/2}$ pollen (Fig. 4n, p, arrowheads).

## Reciprocal translocation associated with the *AtREV3-2* T-DNA insertion

The reduced seed set (but Mendelian distribution of progeny) shown by selfed *AtREV3* $^{+/2}$ heterozygotes, but not *AtREV3* $^{2/2}$ or *AtREV3* $^{+/+}$ homozygotes suggested that a translocation might be associated with the *AtREV3-2* allele. To investigate this possibility, meiotic chromosomes were spread and imaged by epifluorescence microscopy (Fig. 5a–h). In wt Arabidopsis, the five pairs of homologous chromosomes (each chromosome now containing replicated but still cohesed sister-chromatid pairs) became associated at meiosis, forming five structures called bivalents that can be distinguished at diakinesis and metaphase I (Fig. 5a, b). The homologous chromosomes in the bivalents are attached by chiasmata that are the cytological manifestation of cross-overs. In *AtREV3* $^{+/2}$ heterozygotes at diakinesis, four

NIH-PA Author Manuscript

NIH-PA Author Manuscript

NIH-PA Author Manuscript

structures instead of five were observed in 80% of meiocytes ($n$ = 60). Three were bivalent (bv) and one was a tetravalent (tv) containing four chromosomes (Fig. 5c, d). Tetravalent structures are typically formed by cells heterozygous for a reciprocal translocation. In this configuration, a single chromosome can recombine with more than one partner, leading to the formation of multivalent forms whose structures depend on crossover positions.

Could a translocation associated with the *AtREV3-2* allele account for the non-Mendelian distribution of genotypes among progeny of selfed *AtPOLH* $^{+/1}$ *AtREV3* $^{+/2}$ double heterozygotes (Table 1 and Supplementary Table 1)? If the translocation involved both chromosome I and chromosome V, then after abnormal (multivalent) pairing at meiosis I, one mode of segregation would eventually give rise only to inviable gametes (*AtPOLH* $^{+}$ *AtREV3* $^{+}$ or *AtPOLH-1 AtREV3-2*). A different mode would entirely yield viable gametes (*AtPOLH* $^{+}$ *AtREV3-2* or *AtPOLH-1 AtREV3* $^{+}$); see Sect. “Discussion” and Fig. 7. Thus, both double-mutant and double-wt gametes would mostly be lost, consistent with the hypothetical “Expect 2” case (Table 1). To test this hypothesis, we identified the chromosomes involved in the multivalent structures observed during meiosis of *AtREV3* $^{+/2}$ heterozygotes. FISH was performed with a combination of probes that allow the identification of the individual Arabidopsis chromosomes. Tetravalents always involved chromosome I and V, while the other chromosomes (II, III and IV) were always observed as bivalents (Fig. 5g, h). Thus, a translocation involving chromosomes I and V appeared to be associated with insertion of T-DNA at the *AtREV3* locus, perhaps involving a second T-DNA insertion in chromosome V.

## Identification of the junctions of chromosome I DNA and V DNA with inserted T-DNA

We analyzed the products of the hypothesized reciprocal translocation between chromosomes I and V in a series of PCR experiments (Fig. 6). Primer *Ra5′*, specific for Exon 13 of *AtREV3*, was used with a primer specific for the T-DNA left-side (not shown) to amplify a product (p4) that encoded an *AtREV3*-TDNA junction designated J4 (Fig. 6). The J4 junction sequence (Supplementary Table 3) was consistent with the annotation by the Arabidopsis Information Resource (TAIR) of the *AtREV3-2* T-DNA insertion line, SALK_029237. Primer *Rb5′* was used with a series of TDNA-specific primers (not shown) to amplify products that mapped the rightward extent of T-DNA from J4; the longest product (p41) showed this to be at least 4.4 kbp, extending through the right-border (RB) region that is typically transferred into plant DNA (Miranda et al. 1992) (and into a few bp likely to have come from the binary vector used for transformation). Similarly, primer *Ra3′* (also specific for *AtREV3* Exon13) was used with a TDNA (left-side)-specific primer (not shown) to amplify a PCR product (p1) encoding a second *AtREV3*-LB junction, J1 (Supplementary Table 3). *Rb3′* (closer to J1) was used with a series of TDNA-specific primers to map T-DNA at least 3.9 kbp left of J1 (Fig. 6, product p11).

To identify the chromosome V sequences that we expected to be adjacent to TDNA (left-end) sequences, we used “anchored PCR” (O'Malley et al. 2007). We amplified and sub-cloned multiple PCR products using the same “anchored” TDNA-specific primer (not shown) with adaptor primers associated with a *Hin*dIII or an *Eco*RI restriction site, respectively, in adjacent DNA. A major 0.25-kbp product included part of Intron 2 of gene

NIH-PA Author Manuscript

NIH-PA Author Manuscript

NIH-PA Author Manuscript

At5g59220 in chromosome V (Supplementary Table 3), putatively encoding a 2C-type protein phosphatase (provisionally designated AtPP2C), and thus defining junction J2 (Fig. 6). A minor 1.1 kbp product, *not* readily identifiable in the original analytical gel, encoded *AtREV3*Exon13, thus confirming the sequence of junction J1. (Interestingly, a prominent 0.3-kbp anchored-PCR product proved *not* to code any relevant DNA. These results emphasize the importance, in analytical anchored PCR, of subcloning and sequencing a substantial number of PCR products, prominent or not). Finally, primer *P3′*, specific for *AtPP2C* Intron 2, was used with a TDNA-specific primer (not shown) to amplify a product whose sequence identified junction J3 (Supplementary Table 3). The Salk library does not list the insertion in Intron 2 of gene At5g59220 for line SALK_029237, nor do insertions assigned to At5g59220 include the Intron-2 insertion discovered here. Thus, this library most likely contains a great many undiscovered insertion mutations.

We do not know whether the T-DNA insertion in Intron 2 of the putative *AtPP2C* disrupts its function or not. If it does, this function would seem not to be essential, because *AtREV3* $^{2/2}$ mutants, presumably homozygous for the *AtPP2C::TDNA* insertion as well, showed normal growth, development and fertility. In principle, the *AtPP2C::TDNA* mutation might somehow contribute to the UV sensitivity of *AtREV3* $^{2/2}$ mutants (Curtis and Hays 2007). However, Arabidopsis plants homozygous for *AtREV3-3*, a different TDNA-insertion mutation, were shown to be similarly UV-sensitive by Sakamoto et al. (2003). Our observation (data not shown) of normal seed set (similar to wt) by *AtREV3*$^{+/3}$ heterozygotes, unlike *AtREV3* $^{+/2}$ heterozygotes (Table 3), suggests that *AtREV3-3* does *not* involve a translocation.

The evidence for four junctions of T-DNA left ends with Arabidopsis DNA—5′ and 3′ portions of both the *AtREV3* and *AtPP2C* genes—is consistent with an hypothesis of independent compound insertions of T-DNA into these genes. Both insertions are bounded by left-end T-DNA regions inverted with respect to one another (Fig. 6). Our models to explain the genetic analyses (Figs. 7, 8), and the imaging of chromosomal spreads (Fig. 5), are strongly consistent with reciprocal break-and-join events between these two compound T-DNA insertions, likely homologous-recombination cross-overs, that produced the translocations that we suggest in Fig. 6 (lower two structures).

However, no data presented here directly confirm this model. The model predicts that PCR primers that flank T-DNA insertions, encoding CEN-side *AtREV3* DNA and RETEL-side *AtPP2C* DNA (for example, p1a and p2 sequences in Fig. 6) or CEN-side *AtPP2C* and RETEL-side *AtREV3* DNA (for example, p3 and p4 sequences in Fig. 6) should generate large PCR products, containing the inserts. Unfortunately however, one or both insertions appear to include at least one copy of the entire binary vector, which appears to be a far from rare event (Kononov et al. 1997). As noted above, PCR product p41 (Fig. 6), extended through *AtREV3-2* DNA and beyond the RB region into binary-vector sequence. Furthermore, two pairs of PCR primers, encoding binary-vector on each side of the T-DNA, generated robust PCR products when templated by *AtREV3-2* DNA (data not shown). Inserts containing most or all of binary vectors are clearly much too long to be amplified. We also tried to identify a single large restriction fragment in blots of *AtREV3-2* DNA that (within the resolution afforded be gel electrophoresis) would simultaneously hybridize to probes

NIH-PA Author Manuscript

NIH-PA Author Manuscript

NIH-PA Author Manuscript

encoding expected adjacent *AtREV3* and *AtPP2C* DNA. However, we could not interpret the blots in any simple way that unequivocally supported (or falsified) the model shown in Fig. 6, consistent with previous reports of "multiple complex patterns of integration" (Kononov et al. 1997).

## Discussion

The work described here was motivated by outcomes of crosses between two mutant Arabidopsis lines, homozygous for T-DNA insertions that inactivated the *AtPOLH* and *AtREV3* loci, situated on chromosomes V and I, respectively. Selfing of the F1 *AtPOLH* $^{+/1}$ *AtREV3* $^{+/2}$ heterozygotes yielded very few +/++/+ or *1/1 2/2* doubly homozygous F2 progeny—0.42 and 0.25%. Four other F2 genotypes were also underrepresented and three were overrepresented (Table 1, Supplementary Table 1). The entire F2 progeny distribution could be quantitatively explained by the single assumption that selfing of double heterozygotes yielded few double-mutant (*1,2*) or doubly wt (+,+) gametes—each comprising only 6% instead of 25% of the male and female gamete pools. Nevertheless, the normal fertility of (*1/1 2/2*) homozygotes showed that gametes lacking the *AtPOLH* and *AtREV3* gene products (AtPolη and AtPolζ, respectively) are not intrinsically inviable. The properties of single *AtREV3* $^{+/2}$ heterozygotes— 50% reduction in seed set (Table 3), but equal transmission of *AtREV3* $^{+}$ and *AtREV3-2* alleles (Table 4)—are consistent with the hypothesis that T-DNA insertion at the *AtREV3* locus engendered a reciprocal translocation (Patterson 1978). Quantitative light-microscopy of both male and female gametogenesis during selfing of *AtREV3* $^{+/2}$ heterozygotes showed 40–50% of both pollen and ovules to abort or arrest, respectively, after meiosis and fail to enter gametophyte mitosis (Figs. 3, 4). This finding, consistent with the translocation hypothesis, suggested that meiotic segregation produced 50% "sub-haploid" gametophytes, inviable for reasons that have nothing to do with lack of AtREV3 (AtPolζ) activity in the mutant pollen. We define "sub-haploid" gametophytes to lack even one complete copy of some extended block of linked genes.

The markedly non-Mendelian distribution of progeny from selfed A*tPOLH* $^{+/1}$ *AtREV3* $^{+/2}$ double heterozygotes suggested that the putative reciprocal translocation involved the *AtREV3* locus on chromosome I and some site on chromosome V. In fact, the expected cruciform (tetravalent) intermediates were directly observed in chromosome spreads of pollen meiocytes, and FISH showed these to indeed contain I–V translocations (Fig. 5).

Figure 7 suggests how one mode of chromosome segregation ("horizontal"; adjacent segregation) after meiosis I in selfed A*tPOLH* $^{+/1}$ *AtREV3* $^{+/2}$ double heterozygotes might generate "sub-haploid" gametes, lacking one end of chromosome I or chromosome V. The other segregation mode ("diagonal"; alternate segregation) would generate fully haploid and thus functional gametes, although half of these would contain the translocation chromosomes (Patterson 1978). In Fig. 7, the *AtPOLH* locus is assumed to lie on the non-translocated portion of chromosome V. If the *AtPOLH* locus were instead on the translocated portion of chromosome V, "horizontal" segregation would again generate sub-haploid +, + and *1,2*gametes and "diagonal" segregation would again yield fully haploid +,*2* and *1*, + gametes.

NIH-PA Author Manuscript NIH-PA Author Manuscript NIH-PA Author Manuscript

Chromosomal rearrangements are relatively frequent in Arabidopsis transformed by *Agrobacterium*-mediated T-DNA transformation. Castle et al. (1993) observed rearrangements in 7 out of 41 TDNA-tagged mutants. Forsbach et al. (2003) observed translocations in only 2.6% of 112 single-copy T-DNA lines, but chromosomal rearrangements were more frequent in plant lines with more than one T-DNA insertion. Nacry et al. (1998) characterized a reciprocal translocation involving chromosome II and III. In this case there were two independently assorting T-DNA insertions, one T-DNA associated with each breakpoint. On chromosome II, there was also a > 40 kbp inversion associated with T-DNA. Two unilateral translocations were characterized by Tax and Vernon (2001). Each translocation involved only one T-DNA insertion. One involved translocation and duplication of > 40 kbp of chromosome V onto chromosome I. The second translocation involved chromosome V and IV. Lafleuriel et al. (2004) described a reciprocal translocation involving chromosome I and II. These reports focused on molecular characterization of the rearrangements and mechanism of T-DNA integration, but none addressed the stage or stages at which unbalanced gametes become inviable, nor considered the likely effects on progeny distributions involving markers on each of the reciprocally translocated chromosomes. Ray et al. (1997) did analyze gametogenesis in Arabidopsis plants heterozygous for a reciprocal II–V translocation. Approximately 32% of pollen aborted, and female gametophytes arrested at the mononucleate stage (40%) or the binucleate stage (10%), or reached full maturity (50%). Here, we found approximately 50% of female gametophytes generated by *AtREV3* $^{+/2}$ heterozygotes to arrest at the mononucleate stage; the remainder reached maturity. Likewise, approximately 40% of male gametophytes aborted after meiosis but prior to their first mitosis, while the remainder reached maturity. Thus, although half the expected subhaploid gametophytes would lack part of chromosome I and the other half lack part of chromosome V, they all arrested (ovules) or aborted (pollen) shortly after meiosis.

What genes might be lacking in our inferred sub-haploid gametophytes? Of over 100 mutants identified in screens for Arabidopsis deficient in female gametogenesis, twenty show arrest after meiosis at the mononucleate stage (Drews and Yadegari 2002). Pagnussat et al. (2005) identified 42 mutants defective in female gametogenesis. Of these, only one mutant (mutation on chromosome IV) arrested at the mononucleate stage. In contrast, Christensen et al. (2002) found 13 of 39 gametophytic mutants to arrest at the female mononucleate stage. Six of these 13 mutants showed roughly similar effects on male and female gametogenesis. Where were the mutations located? *Fem-3* is on chromosome I, but not in the region that is deficient or duplicated by the reciprocal translocation in our study. *Ata-4* is on chromosome III. The chromosomal locations of four of these mutants, *fem-12,35,37* and *gfa5* are not known. Of the remainder of the 20 mutants showing arrest at the female mononucleate stage, the *gf* mutant isolated by Redei (1965) is on chromosome II, and the remaining five mutants show embryo sac degeneration. In our studies, the putative sub-haploid gametophytes lack either chromosome I or chromosome V genes, but *both* types arrested at the mononucleate stage without embryo sac degeneration. Thus, one of the four genes (*FEM-12,35,37* or *GFA5*) for which the chromosomal locations are not known may be located in the chromosome I region that is missing in half the sub-haploid gametophytes. A

NIH-PA Author Manuscript

NIH-PA Author Manuscript

NIH-PA Author Manuscript

second such gene located in the chromosome V region might be missing from the other half, or other genes not yet identified by mutation might be missing.

Alternatively, we speculate that a general post-meiotic checkpoint might be sensitive to the presence of chromosome deletions or duplications, thus ensuring elimination of aberrant gametes from pre-fertilization pools. (Gametes subhaploid for one chromosome would be "supra-haploid" for another, Fig. 7). A study by Henry et al. (2007) does suggest a possible genetic modifier of aneuploid survival, the Sensitive to Dosage Imbalance (*SDI*) locus. However, it is not known at what stage of haploid or diploid development *SDI* affects aneuploid survival. Whatever the mechanism, the genotype-specific gametophyte lethality seen here was not total. The skewed distribution of genotypes among F2 progeny of selfed double heterozygotes could be explained quantitatively by assuming that roughly 1/7 of putative sub-haploid (*1*,*2*) and (+,+) gametophytes escaped lethality. Alternatively, if meiotic recombination rearranged 2/7 of the tetravalent cruciforms, as suggested at the top of Fig. 8a, then "diagonal" segregation would yield 1/7 of the time euploid (+,+) and (*1*,*2*) gametophytes, each containing one recombinant chromosome (X). This would account for the F2 progeny distribution.

We previously observed normal Mendelian distribution of the F3 progeny of selfed F2 *AtPOLH* $^{1/1}$ *AtREV3*$^{+/2}$ and *AtPOLH* $^{+/1}$ *AtREV3* $^{2/2}$ plants (Curtis and Hays 2007). This appears more consistent with the suggested meiotic crossovers during the selfing of F1 double-heterozygotes (Fig. 8a) than partial escape of subhaploid gametophytes from lethality, as follows. The *1/1 +/2* and *+/1 2/2* F2 plants, which were themselves underrepresented (relative to Mendelian expectations), would not have been present at all if some (*1*,*2*) gametophytes had not matured. If the (*1/1 +/2*) F2 plants, for example, resulted from F1 recombination (X), as shown in the upper left corner of Fig. 8b, then meiosis I tetravalents would again form during F2 selfing. These would yield 1/2 euploid gametophytes and 1/2 sub-haploid gametophytes, depending on the mode of segregation during meiosis I (Fig. 8b, lower left corner). Of the euploid gametophytes, 50% would be (*1*, +) and 50% would be (*1*,*2*); selfing would yield the observed Mendelian F3 progeny distribution (25% (*1/1 2/2*)). As also predicted, the total seed sets of selfed F2 *AtPOLH* $^{1/1}$ *AtREV3* $^{+/2}$ plants were 50% of normal (data not shown). However, if the (*1/1 +/2*) F2 plants resulted from lethality escape during the F1 selfing, and were thus themselves aneuploid (Fig. 8b, upper right corner), then one normal and one abnormal bivalent would form during meiosis I. Gametophyte maturation would produce mostly (*1*, +) euploid gametophytes, plus perhaps a few (*1*,*2*) sub-haploid gametophytes that again escaped lethality (Fig. 8b, lower right corner). Most F3 progeny would therefore be (*1/1* +/+), contrary to observation (Curtis and Hays 2007).

## Conclusion

Most constructions of Arabidopsis double or triple mutants begin with one or more TDNA-insertion mutations. However, TDNA-induced chromosomal rearrangements, which are relatively frequent [up to 17% of T-DNA lines; Castle et al. (1993)], may interfere with these constructions. If non-Mendelian segregation is observed among F2 progeny from selfed F1 plants doubly heterozygous for two TDNA-insertion mutations, we suggest

NIH-PA Author Manuscript

NIH-PA Author Manuscript

NIH-PA Author Manuscript

immediate checking of the single-insertion heterozygotes for reduced seed set—an indicator of the presence of a translocation (Patterson 1978). Where several TDNA-insertion mutations for a single locus are available, it might be advantageous to compare their seed sets at the beginning. If the entire non-Mendelian F2 progeny distribution can be quantitatively accounted for simply by assuming loss of double-mutant and double-wild type gametes, then a reciprocal translocation involving the two chromosomes harboring the respective T-DNA insertions would seem likely. Under these circumstances, the double mutant may nevertheless be efficiently isolated by selfing the appropriate F2 (−/− +/−) plant. Our observations suggest that this F2 parent would be derived from the union of a non-recombinant gamete with a recombinant gamete (Fig. 8b, F1-recombinant progeny), and that all of its F3 progeny would be genetically balanced.

Multiple T-DNA insertions are likely to be quite frequent in Arabidopsis TDNA-insertion libraries (Humann et al. 2006; Jorgensen et al. 1986; Lee et al. 2003; Viss et al. 2003). Insertions of inverted T-DNA repeats are common (Jorgensen et al. 1986) and two or more of these will provide extended regions for homologous recombination regardless of the respective directions of insertion into plant DNA. These may often be the source of reciprocal translocations, which could presumably occur at anytime during continued propagation of a particular line. Thus, multiple T-DNA insertions should be segregated away from one another. If it is necessary to use multiple-insertion lines in experiments, investigators should be alert to the possibility that de novo translocations are possible. It seems particularly important to segregate additional insertion loci away from TDNA-insertion mutations used to construct multiply marked lines.

## Supplementary Material

Refer to Web version on PubMed Central for supplementary material.

## Acknowledgments

This work was supported by National Science Foundation grant MCB 03455001 to J.B.H. We thank Dr. Jennifer Lorang and Buck Wilcox for critical reading of the manuscript, and Dr. Walter Ream for helpful general information about TDNA insertions.

## Abbreviations

| | |
|---|---|
| **UV-B** | Ultraviolet radiation B |
| **T-DNA** | Transferred DNA of the tumor-inducing plasmid |
| **wt** | Wild-type |
| **TAIR** | Arabidopsis information resource |
| **FISH** | Fluorescence in situ hybridization |
| **RB** | T-DNA right border |
| **LB** | T-DNA left border |
| **CEN** | Centromere |

NIH-PA Author Manuscript

NIH-PA Author Manuscript

NIH-PA Author Manuscript

| | |
|---|---|
| **LETEL** | Left telomere |
| **RETEL** | Right telomere |

## References


Campell BR, Song Y, Posch TE, Cullis CA, Town CD. Sequence and organization of 5S ribosomal RNA-encoding genes of *Arabidopsis thaliana*. Gene. 1992; 112:225–228. [PubMed: 1348233]

Castle LA, Errampalli D, Atherton TL, Franzmann LH, Yoon ES, Meinke DW. Genetic and molecular characterization of embryonic mutants identified following seed transformation in *Arabidopsis*. Mol Gen Genet. 1993; 241:504–514. [PubMed: 8264525]

Christensen CA, Gorsich SW, Brown RH, Jones LG, Brown J, Shaw JM, Drews GN. Mitochondrial GFA2 is required for synergid cell death in Arabidopsis. Plant Cell. 2002; 14:2215–2232. [PubMed: 12215516]

Curtis MJ, Hays JB. Tolerance of dividing cells to replication stress in UVB-irradiated Arabidopsis roots: requirements for DNA translesion polymerases eta and zeta. DNA Repair (Amst). 2007; 6:1341–1358. [PubMed: 17482896]

Drews GN, Yadegari R. Development and function of the angiosperm female gametophyte. Annu Rev Genet. 2002; 36:99–124. [PubMed: 12429688]

Drews GN, Lee D, Christensen CA. Genetic analysis of female gametophyte development and function. Plant Cell. 1998; 10:5–18. [PubMed: 9477569]

Forsbach A, Schubert D, Lechtenberg B, Gils M, Schmidt R. A comprehensive characterization of single-copy T-DNA insertions in the *Arabidopsis thaliana* genome. Plant Mol Biol. 2003; 52:161–176. [PubMed: 12825697]

Gerlach WL, Bedbrook JR. Cloning and characterization of ribosomal RNA genes from wheat and barley. Nucleic Acids Res. 1979; 7:1869–1885. [PubMed: 537913]

Grelon M, Vezon D, Gendrot G, Pelletier G. AtSPO11–1 is necessary for efficient meiotic recombination in plants. EMBO J. 2001; 20:589–600. [PubMed: 11157765]

Henry IM, Dilkes BP, Comai L. Genetic basis for dosage sensitivity in *Arabidopsis thaliana*. PLoS Genet. 2007; 3:e70. [PubMed: 17465685]

Honys D, Twell D. Transcriptome analysis of haploid male gametophyte development in *Arabidopsis*. Genome Biol. 2004; 5:R85. [PubMed: 15535861]

Humann J, Andrews S, Ream W. VirE1-mediated resistance to crown gall in transgenic *Arabidopsis thaliana*. Phytopathology. 2006; 96:105–110. [PubMed: 18944210]

Jorgensen R, Snyder C, Jones JDG. T-DNA is organized predominantly in inverted repeat structures in plants transformed withAgrobacterium tumefaciens C58 derivatives. Mol Gen Genet. 1986; 207:471–477.

Kononov ME, Bassuner B, Gelvin SB. Integration of T-DNA binary vector ‘backbone’ sequences into the tobacco genome: evidence for multiple complex patterns of integration. Plant J. 1997; 11:945–957. [PubMed: 9193068]

Lafleuriel J, Degroote F, Depeiges A, Picard G. A reciprocal translocation, induced by a canonical integration of a single T-DNA, interrupts the HMG-I/Y *Arabidopsis thaliana* gene. Plant Physiol Biochem. 2004; 42:171–179. [PubMed: 15051040]

Laufs P, Autran D, Traas J. A chromosomal paracentric inversion associated with T-DNA integration in Arabidopsis. Plant J. 1999; 18:131–139. [PubMed: 10363366]

Lee H, Humann JL, Pitrak JS, Cuperus JT, Parks TD, Whistler CA, Mok MC, Ream LW. Translation start sequences affect efficiency of silencing of *Agrobacterium tumefaciens* T-DNA oncogenes. Plant Physiol. 2003; 133:966–977. [PubMed: 12972655]

Lysak M, Fransz P, Schubert I. Cytogenetic analyses of Arabidopsis. Methods Mol Biol. 2006; 323:173–186. [PubMed: 16739577]

NIH-PA Author Manuscript

NIH-PA Author Manuscript

NIH-PA Author Manuscript

Miranda A, Janssen G, Hodges L, Peralta EG, Ream W. *Agrobacterium tumefaciens* transfers extremely long T-DNAs by a unidirectional mechanism. J Bacteriol. 1992; 174:2288–2297. [PubMed: 1551847]

Nacry P, Camilleri C, Courtial B, Caboche M, Bouchez D. Major chromosomal rearrangements induced by T-DNA transformation in Arabidopsis. Genetics. 1998; 149:641–650. [PubMed: 9611180]

O'Malley RC, Alonso JM, Kim CJ, Leisse TJ, Ecker JR. An adapter ligation-mediated PCR method for high-throughput mapping of T-DNA inserts in the *Arabidopsis* genome. Nat Protoc. 2007; 2:2910–2917. [PubMed: 18007627]

Pagnussat GC, Yu HJ, Ngo QA, Rajani S, Mayalagu S, Johnson CS, Capron A, Xie LF, Ye D, Sundaresan V. Genetic and molecular identification of genes required for female gametophyte development and function in *Arabidopsis*. Development. 2005; 132:603–614. [PubMed: 15634699]

Patterson, EB. Properties and uses of duplicate-deficient chromosome complements in maize.. In: Walden, DB., editor. Maize breeding and genetics. Wiley-Interscience; New York: 1978. p. 693-710.

Ray SM, Park SS, Ray A. Pollen tube guidance by the female gametophyte. Development. 1997; 124:2489–2498. [PubMed: 9199374]

Redei GP. Non-Mendelian megagametogenesis in Arabidopsis. Genetics. 1965; 51:857–872. [PubMed: 17248261]

Rine J. Cell biology. Twists in the tale of the aging yeast. Science. 2005; 310:1124–1125.

Sakamoto A, Lan VT, Hase Y, Shikazono N, Matsunaga T, Tanaka A. Disruption of the *AtREV3* gene causes hypersensitivity to ultraviolet B light and gamma-rays in *Arabidopsis*: implication of the presence of a translesion synthesis mechanism in plants. Plant Cell. 2003; 15(9):2042–2057. [PubMed: 12953110]

Schneitz K, Hulskamp M, Pruitt RE. Wild-type ovule development in *Arabidopsis thaliana*: a light microscope study of cleared whole-mount tissue. Plant J. 1995; 7:731–749.

Siddiqi I, Ganesh G, Grossniklaus U, Subbiah V. The dyad gene is required for progression through female meiosis in Arabidopsis. Development. 2000; 127:197–207. [PubMed: 10654613]

Tax FE, Vernon DM. T-DNA-associated duplication/translocations in Arabidopsis. Implications for mutant analysis and functional genomics. Plant Physiol. 2001; 126:1527–1538. [PubMed: 11500551]

Viss WJ, Pitrak JS, Humann J, Cook M, Driver J, Ream W. Crown-gall-resistant transgenic apple trees that silence *Agrobacterium tumefaciens* oncogenes. Mol Breed. 2003; 12:283–295.

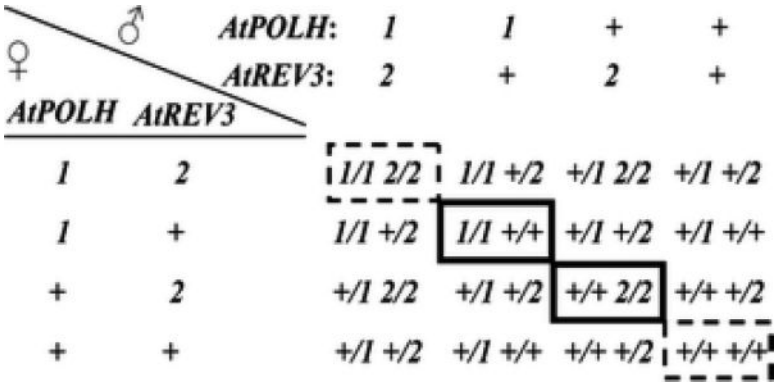


**Fig. 1.**

Expected F2 progeny from selfed F1 parents heterozygous at two independent loci. Progeny that derive solely from unions of gametes that are each mutant at one locus but wt at the other (*AtPOLH* + *AtREV3-2*and *AtPOLH-1 AtREV3* +) are enclosed by the *solid-line box*. Progeny derived solely from unions of gametes that are both double-mutant and/or double-wt (*AtPOLH-1 AtREV3-2* and *AtPOLH* + *AtREV3* +) are enclosed by the *dashed-line boxes*



NIH-PA Author Manuscript NIH-PA Author Manuscript NIH-PA Author Manuscript

NIH-PA Author Manuscript

NIH-PA Author Manuscript

NIH-PA Author Manuscript

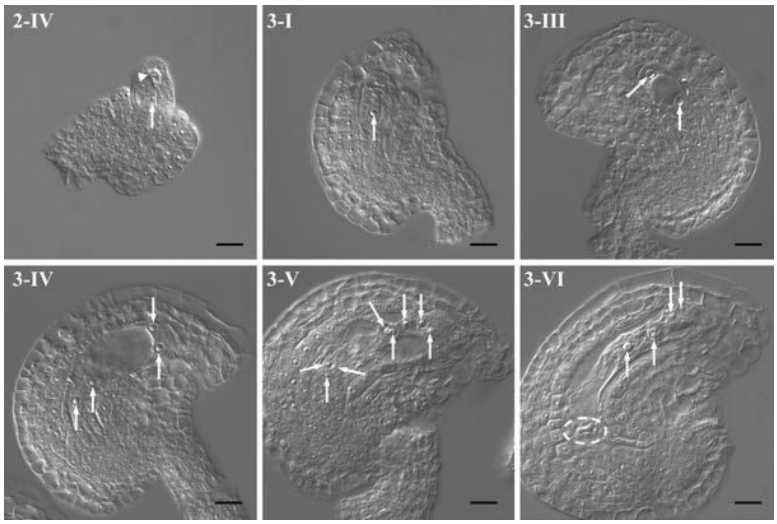


**Fig. 2.**

Whole-mount microscopy of developmentally staged ovules. Ovules were dissected from fixed and cleared ovaries as described under Sect. “Materials and methods”, and imaged by differential-interference microscopy. Stages of development are those defined by Schneitz et al. (1995). *Stage 2-IV arrow* indicates nucleus of spore selected to undergo gametogenesis. *Stage 3-I arrow* indicates nucleus of growing gamete. (*Stage 3-II*, after the first mitosis but before the embryo sac vacuole forms, is not shown here.) *Stage 3-III arrows* indicate nuclei derived from first gamete mitosis. The embryo sac vacuole is now obvious. *Stage 3-IV arrows* indicate nuclei derived from second gamete mitosis. *Stage 3-V arrows* indicate nuclei derived from third gamete mitosis. *Stage 3-VI arrows*, from *left* to *right*, indicate nuclei of the central cell, egg cell and synergids, respectively. *Dashed circle* surrounds the three degenerate antipodal cells. All panels have the same magnification. *Bar* 10 μm

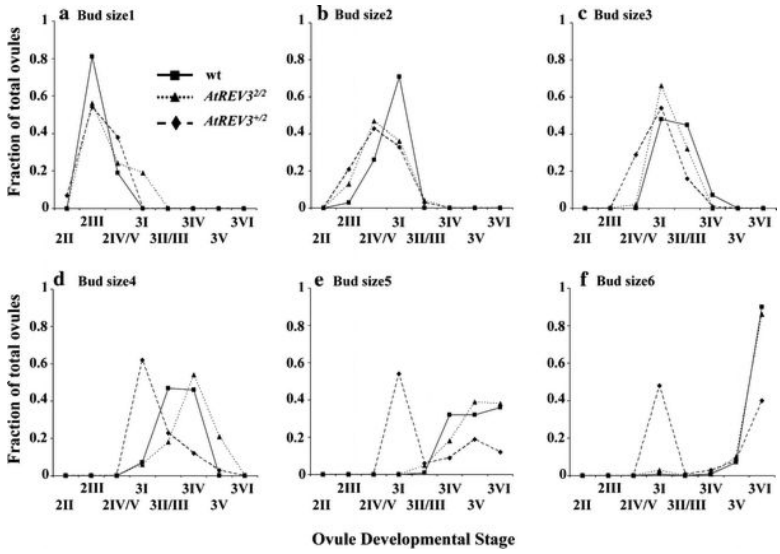


**Fig. 3.**

**a–f** Ovule development in consecutive buds from wt, *AtREV3* $^{2/2}$ and *AtREV3* $^{+/2}$ inflorescence. Buds of size no. 1 are the youngest dissected; buds of size no. 6 are the most mature. Stages of ovule development were scored as described in the legend of Fig. 2. The fraction of total ovules at each developmental stage was determined for each consecutive sets of buds, by taking the sum of ovules at each stage and dividing by the total; three wt, three *AtREV3* $^{2/2}$ and five *AtREV3* $^{+/2}$ inflorescences were analyzed. (Supplementary Figures 1, 2, 3 show distributions for individual buds). Total ovules scored for bud sizes no. 1–6, respectively, were as follows: wild-type, 63, 83, 100, 68, 76 and 70 ($n$ = 3); *AtREV3* $^{2/2}$, 78, 94, 113, 107, 65 and 70 ($n$ = 3); *AtREV3* $^{2/+}$ , 68, 135, 175, 164, 183 and 192 ($n$ = 5)



NIH-PA Author Manuscript NIH-PA Author Manuscript NIH-PA Author Manuscript

NIH-PA Author Manuscript

NIH-PA Author Manuscript

NIH-PA Author Manuscript

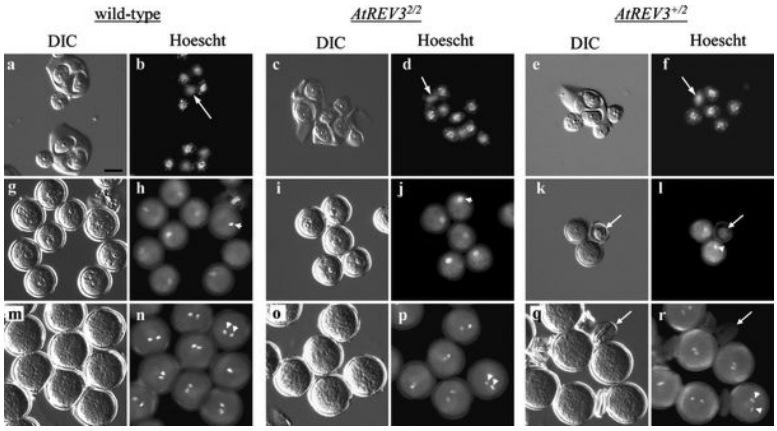


**Fig. 4.**

Pollen development imaged by microscopy. Pollen was dissected out of single anthers, after fixing primary inflorescences and overnight staining of flower buds with Hoechst dye, as described under Sect. “Materials and methods”. Pollen was imaged by differential-interference (*DIC*) or epifluorescence (Hoechst) microscopy. **a–f** Tetrads dissected out of anthers from indicated genotype. *Arrows* indicate Hoechst-stained nuclei. **g–l** Pollen, after vacuole absorption, dissected out of anthers from indicated genotype. *Arrowheads* indicate single Hoechst-stained pollen nuclei. *Arrows* in panels **k** and **l** indicate degenerating pollen. **m–r** Pollen after first gamete mitosis. *Arrowheads* in panels **n**, **p** and **r** indicate two Hoechst-stained pollen nuclei. *Arrows* in panels **q** and **r** indicate degenerated pollen. Images are representative of two, three and four wild-type, *AtREV3* $^{2/2}$ and *AtREV3* $^{2/+}$ plants, respectively. All panels show the same magnification. *Bar* 20 μm

NIH-PA Author Manuscript
NIH-PA Author Manuscript
NIH-PA Author Manuscript



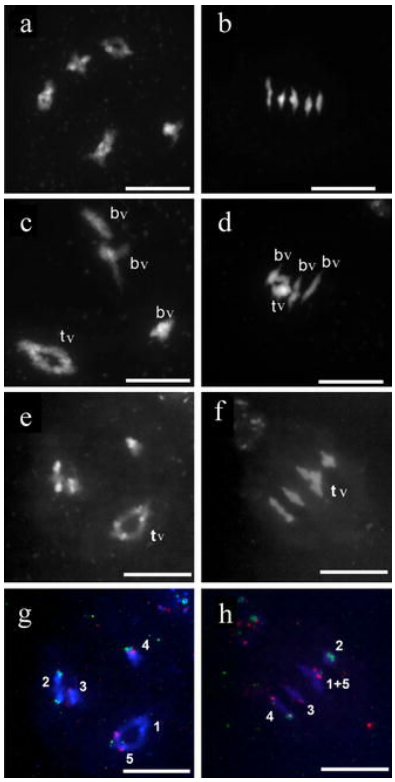


**Fig. 5.**

Imaging of chromosome spreads and fluorescence in situ hybridization (FISH) of Arabidopsis meiocytes. Meiocytes from wild-type (**a**, **b**) and *AtREV3* $^{+/2}$ (**c–h**) plants were isolated and chromosomes spread, stained and imaged as described under Sect. “Materials and methods”. Imaging of wild-type meiocytes at meiosisdiakinesis (**a**) and metaphase I (**b**). Imaging of *AtREV3* $^{+/2}$ meiocytes at meiosisdiakinesis (**c**, **e**) and metaphase I (**d**, **f**). *bv* Bivalent, *tv* tetravalent. **g**, **h** FISH of meiocytes shown in **e** and **f**, respectively. For clarity in **g** and **h**, chromosomes I, II,…V are indicated by the corresponding Arabic numerals 1, 2,… 5. Chromosomes I through V were identified by chromosome-specific FISH: no signal, chr. I; strong *green* signal (25S rDNA), chr. II; *red* signals (5S rDNA and BACS F8J2 and T4P13), chr. III; adjacent *red* and *green* (5S and 25S rDNA), chr. IV; strong *red* signal (5S rDNA) and faint *green* signal (BACS F7J8 and F2I11), chr. V. Note that chromosomes I and V are always associated with the tetravalent (*tv*). *Bar* 10 μm

NIH-PA Author Manuscript

NIH-PA Author Manuscript

NIH-PA Author Manuscript

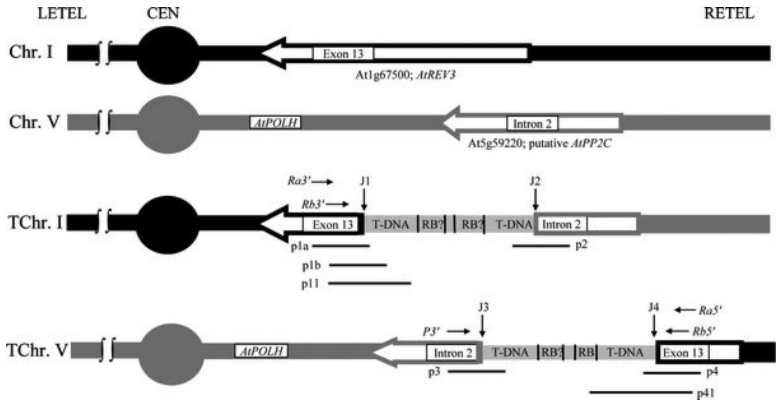


**Fig. 6.**

Structures of translocation-rearranged T-DNAs in Arabidopsis chromosomes I and V. *Upper* structures, native chromosomes I (*black shading*) and V (*darker-gray shading*), not drawn to scale. Centromeres (*filled circles*) and *left* and *right* chromosome ends (telomeres; LETEL and RETEL) are oriented as in the TAIR representations. The genes involved in the translocation, *AtREV3* (Exon 13) and putative *AtPP2C*(Intron 2) are indicated by *black-outlined* or *darker-gray-outlined large arrows*, respectively. Transcription of both genes is *right* (5′) to *left* (3′) as shown, i.e., sense strands (3′–5′, CEN to RETEL direction) are on the *bottom*. The position of *AtPOLH* relative to *AtPP2C* and the chromosome V centromere is indicated.*Lower* structures. Inferred RETEL ends of translocation chromosomes (TChr. I and TChr. V). *Light-gray*-shaded areas contain indicated components of compound T-DNA insertions in both Chr. I and Chr. V, each containing at least two T-DNA *left* sides which are inverted with respect to one another in both cases. Thus, T-DNA *left* sides flank both sides of both insertion structures. The presence of one corresponding *right* border (*RB*) has been confirmed (see below). Whether others (RB?) are present as well has not been determined. Reciprocal translocation is suggested to have occurred via homologous recombination between the two compound T-DNA insertions (see text). *Horizontal arrows* above *top* strands indicate four primers specific for indicated regions of *AtREV3* Exon13 (*Ra5′* and *Rb5′*, *Ra3′* and*Rb3′*, complementary to the indicated *top* and *bottom* strands, respectively) and one specific for *AtPP2C* Intron 2 (*P3′*, complementary to the *bottom* strand). *Vertical arrows* indicate junctions between *AtREV3*and *left*-end TDNA (J1, J4) and between *AtPP2C* and left-end TDNA (J2, J3). The J4 sequence was determined from a PCR product (p4) amplified using *Ra5′*, and a TDNA-specific primer (not shown). The extension of TDNA from J1 through the RB terminus (4.4 kbp) was determined using *Rb5′* plus various other TDNA-specific primers (not shown) to amplify a series of products, of which p41 was the longest. The J3 sequence was determined from product p3, amplified using primer *P3′* and one TDNA-specific primer (not shown). The J2 sequence was obtained from one product (p2) of “anchored PCR” using a TDNA-specific “anchored” primer (not shown); see text. The J1 junction was determined from PCR product p1a, amplified using primer *Ra3′* and a TDNA-specific primer (not shown) and was confirmed by product p1b from the same anchored-PCR experiment that identified J2. The extension of the T-DNA at least as far as 3.9-kbp from J1 was demonstrated by PCR amplification (product p11) using *Rb3′* and a TDNA-specific primer (not shown)

NIH-PA Author Manuscript

NIH-PA Author Manuscript

NIH-PA Author Manuscript

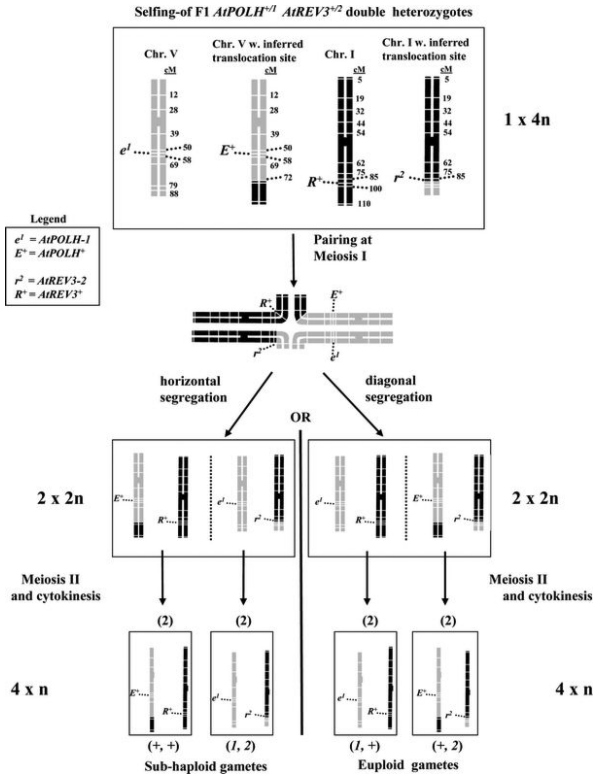


**Fig. 7.**

Inferred pathway for translocation-perturbed selfing of F1 plants doubly heterozygous for TDNA-insertion mutations. *Top box* encloses chromosome I and V structures in selfing F1 *AtPOLH* $^{+/1}$ *AtREV3* $^{+/2}$ plants and shows the relative locations of the *AtPOLH* and *AtREV3* loci on the Arabidopsis genetic map; *cM*centimorgans. Pairing at meiosis I results in a tetravalent (cruciform) structure. Two modes of segregation are possible. *Horizontal* segregation (adjacent segregation) would yield 2 × 2*n* bivalents (*left*) which meiosis II and cytokinesis convert into two sets of two each (+,+) and (*1*,*2*) sub-haploid gametophytes, lacking part of chromosome V but partially duplicated for chromosome I or lacking part of chromosome I but partially duplicated for chromosome V, respectively. Diagonal segregation (alternate segregation) would yield 2 × 2*n* bivalents which give rise to (*1*,+) and (+*2*) gametophytes

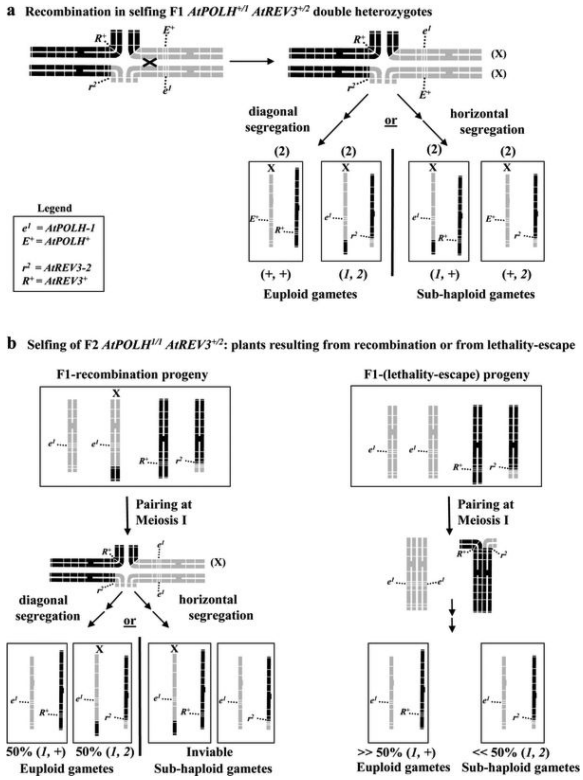


**Fig. 8.**

Models to explain Mendelian distribution of progeny of selfed F2 *AtPOLH* $^{1/1}$ *AtREV3* $^{+/2}$ plants. **a**Outcome of meiotic recombination in selfing F1 *AtPOLH* $^{+/1}$ *AtREV3* $^{+/2}$ plants. If a cross-over occurred in the region between the *AtPOLH* locus and the translocation breakpoint, then two recombinant chromosomes (X) would arise: the *AtPOLH* $^{+}$ allele now on a normal chromosome V and the *AtPOLH-1*allele now linked to the translocation chromosome V. Diagonal segregation (*left*) would give rise eventually to four euploid gametes of two types, wt (+,+) or double mutant (*1 2*). Horizontal segregation (right) would give rise to sub-haploid gametophytes that do not mature into gametes. **b** Alternative outcomes in selfing of F2 *AtPOLH* $^{1/1}$ *AtREV3* $^{+/2}$ plants, themselves the result of recombination or lethality escape during F1 selfing. F1 recombination would yield F2 *AtPOLH* $^{1/1}$ *AtREV3* $^{+/2}$ parents derived by the F1 unions of (*1*,+) gametes with rare recombinant (*1*,*2*) gametes. Pairing at meiosis I would yield tetravalents and diagonal segregation eventually would give rise to equal numbers of viable, euploid (*1*,+) and (*1 2*) gametes. In contrast, the F2 *AtPOLH* $^{1/1}$ *AtREV3* $^{+/2}$ parent might be derived by F1 unions of (*1*,+) gametes with occasional sub-haploid (*1*,*2*) gametes that had escaped lethality. Pairing at meiosis I would yield only bivalents. Their independent assortment would mostly give rise to mostly viable euploid (+,*1*) gametes, plus perhaps a few (*1*,*2*) gametes that again escaped lethality



NIH-PA Author Manuscript NIH-PA Author Manuscript NIH-PA Author Manuscript

NIH-PA Author Manuscript

NIH-PA Author Manuscript

NIH-PA Author Manuscript

## Table 1

Non-Mendelian segregation in F2 progeny of selfed *AtPOLH*$^{+/1}$ *AtREV3*$^{+/2}$ F1 heterozygotes

| F2 Progeny genotype[a] | | Obs.[b] (freq.) | Expect 1[c] (freq.) | Expect 2[d] (freq.) |
|---|---|---|---|---|
| ***AtPOLH*** | ***AtREV3*** | | | |
| 1/1 | 2/2 | 2 (0.005) | 27 (0.062) | 2 (0.004) |
| +/1 | 2/2 | 20 (0.05) | 54 (0.125) | 23 (0.053) |
| +/+ | 2/2 | 66 (0.15) | 27 (0.062) | 83 (0.195) |
| 1/1 | +/2 | 24 (0.06) | 54 (0.125) | 23 (0.053) |
| +/1 | +/2 | 173 (0.40) | 108 (0.25) | 168 (0.39) |
| +/+ | +/2 | 24 (0.06) | 54 (0.125) | 23 (0.053) |
| 1/1 | +/+ | 90 (0.21) | 27 (0.062) | 83 (0.195) |
| +/1 | +/+ | 29 (0.07) | 54 (0.125) | 23 (0.053) |
| +/+ | +/+ | 2 (0.005) | 27 (0.062) | 2 (0.004) |

[a] *AtREV3-2* and *AtPOLH-1* alleles contain a T-DNA insertion. + indicates wild-type alleles

[b] Observed number of respective genotypes determined by PCR analysis of F2 progeny, as described under Sect. “Materials and methods”

[c] Expected progeny distribution for Mendelian segregation of two independent loci. Chi-square test of observed distribution: $\chi^2 = 355.0$; for degrees freedom = 8, $P < 0.005$

[d] Expected progeny distribution for segregation when *AtPOLH* + *AtREV3* + and *AtPOLH-1 AtREV3-2*gamete frequencies are each reduced from 0.25 (normal) to 0.06 of total gametes. Chi-square test of observed distribution: $\chi^2 = 8.16$; for degrees freedom = 8, $P > 0.10$

NIH-PA Author Manuscript

NIH-PA Author Manuscript

NIH-PA Author Manuscript

## Table 2

Summed allele combinations observed at *AtREV3* or *AtPOLH* loci among all progeny of a selfed F1*AtPOLH*$^{+/1}$ *AtREV3*$^{+/2}$ double heterozygote

| | ***AtREV3*** | | | **Total (*2*), (+)** | ***AtPOLH*** | | | **Total (*1*), (+)** |
|---|---|---|---|---|---|---|---|---|
| | ***2/2*** [a] | ***+/2*** | +/+ | | ***1/1*** [a] | ***+/1*** | +/+ | |
| Observed | 88 | 221 | 121 | 397, 463 | 116 | 222 | 92 | 454, 406 |
| Expected[b] | 108 | 215 | 108 | 431, 431 | 108 | 215 | 108 | 431, 431 |

[a] *AtREV3-2* and *AtPOLH-1* alleles contain a T-DNA insertion. + indicates the wild-type allele

[b] Expected progeny distribution for Mendelian segregation of a single locus. Chi-square test shows differences between observed versus expected distributions to not be significant: for *AtREV3*, $\chi^2 = 5.3$, $P > 0.5$; for *AtPOLH*, $\chi^2 = 3.2$, $P > 0.1$

NIH-PA Author Manuscript

NIH-PA Author Manuscript

NIH-PA Author Manuscript

## Table 3

Fertility (seed set) of indicated parents

| *AtREV3* | *N* [a] | Mean seeds | Siliques with | |
|---|---|---|---|---|
| | | Per (*n*) total siliques | <35 Seeds | >35 Seeds |
| *2/2* | 12 | 46 ± 6.2 (*59*) | 3 (1/5, 2/5) | 56 |
| *+/2* | 27 | 25 ± 4.2[b] (*135*) | 135 (all 5/5) | 0 |
| +/+ | 9 | 50 ± 5.1 (*43*) | 0 (all 0/5) | 43 |

[a] Number of plants (4–5 siliques scored per plant)

[b] Significantly (Student's *t*-test) different from +/+ and *2/2* mean

NIH-PA Author Manuscript

NIH-PA Author Manuscript

NIH-PA Author Manuscript

## Table 4

Progeny genotypes segregating from a selfed *AtREV3*$^{+/2}$ heterozygote

| *AtREV3* | Observed (%) | Expected (%) |
|---|---|---|
| *2/2* | 64 (24) | 66 (25) |
| *+/2* | 120 (45) | 132 (50) |
| +/+ | 81 (31) | 66 (25) |

$P \approx 0.1$ for observed versus expected (Chi-square test): not significantly different